Czech Technical University in Prague
Faculty of Nuclear Sciences and Physical Engineering

Study of Jets Containing Beauty Quark in ALICE Experiment

Research

Supervisor: Mgr. Jaroslav Bielčík, PhD.
Advisor: RNDr. Jana Bielčíková, PhD.

Prague, 2009

Michal Vajzer

Table of Contents

List of Figures

List of Tables

Introduction

In this work, I want to investigate, how well does reconstructed jet-cone follow direction of original b-quark. Also, because 20% of mesons containing beauty quark decay through channel, where at least one lepton is present, I want to investigate what information we can obtain from this electron, for example about direction of beauty quark, therefore, how well does it follow axis of reconstructed jet.

Firstly, I will discuss tracking, tagging, track identification capabilities of ALICE experiment with added section on jet reconstruction algorithm, and subsequently proceed to results obtained from simulated and reconstructed sample in official ALICE software, AliRoot.

Chapter 1

Experimental framework

1.1 ALICE experiment

ALICE (A Large Ion Collider Experiment) is multi-purpose heavy-ion colliding experiment, one of LHC's main experiments, intended for study of strongly interacting matter and quark-gluon plasma. Additionally it shall provide reference data from proton - proton and proton - nucleus collisions It's designed to deal with high particle multiplicities anticipated in lead - lead collisions.

ALICE, Fig. 1.1, consists of central detection system inside solenoid magnet of up to 0.5T. This is composed of Inner Tracking System, ITS, Time Projection Chamber, TPC, Transition Radiation Detector, TRD, and Time-of-Flight detector,TOF. Complement to these central detectors in $\mid \eta \mid \leq 0.9$ and full azimuthal angle are cherenkov detectors in High-Momentum Particle Identification Detector, HMPID, with $\mid \eta \mid \leq 0.6$ and 57.6° azimuthal coverage, and ElectroMagnetic Calorimeter, EMCal, with 100° azimuthal coverage at $\mid \eta \mid \leq 0.12$ and Photon Spectrometer, PHOS. At large rapidities are placed Photon Multiplicity Detector, PMD, Forward Multiplicity Detector, FMD, and muon spectrometer. Additional systems include V0 and T0 system for faster triggering and Zero Degree Calorimeter, ZDC.*

1.2 Tagging

Tagging of beauty quark and hadron is done by secondary vertex reconstruction. This is possible, because mesons from b-quark live long time and may travel several hundreds of micrometers from primary vertex, point of collision between protons, before decay. Also because B - mesons have branching ratio of nearly 20% through channels containing lepton, high momenta electrons originating in secondary vertex are used as a trigger. For this purpose, particle identification and tracking are necessary. In this work, I will limit myself to central region, where identification and tracking is carried by ITS, TPC, TRD and TOF.

*Data are from [1], [2] and [3].

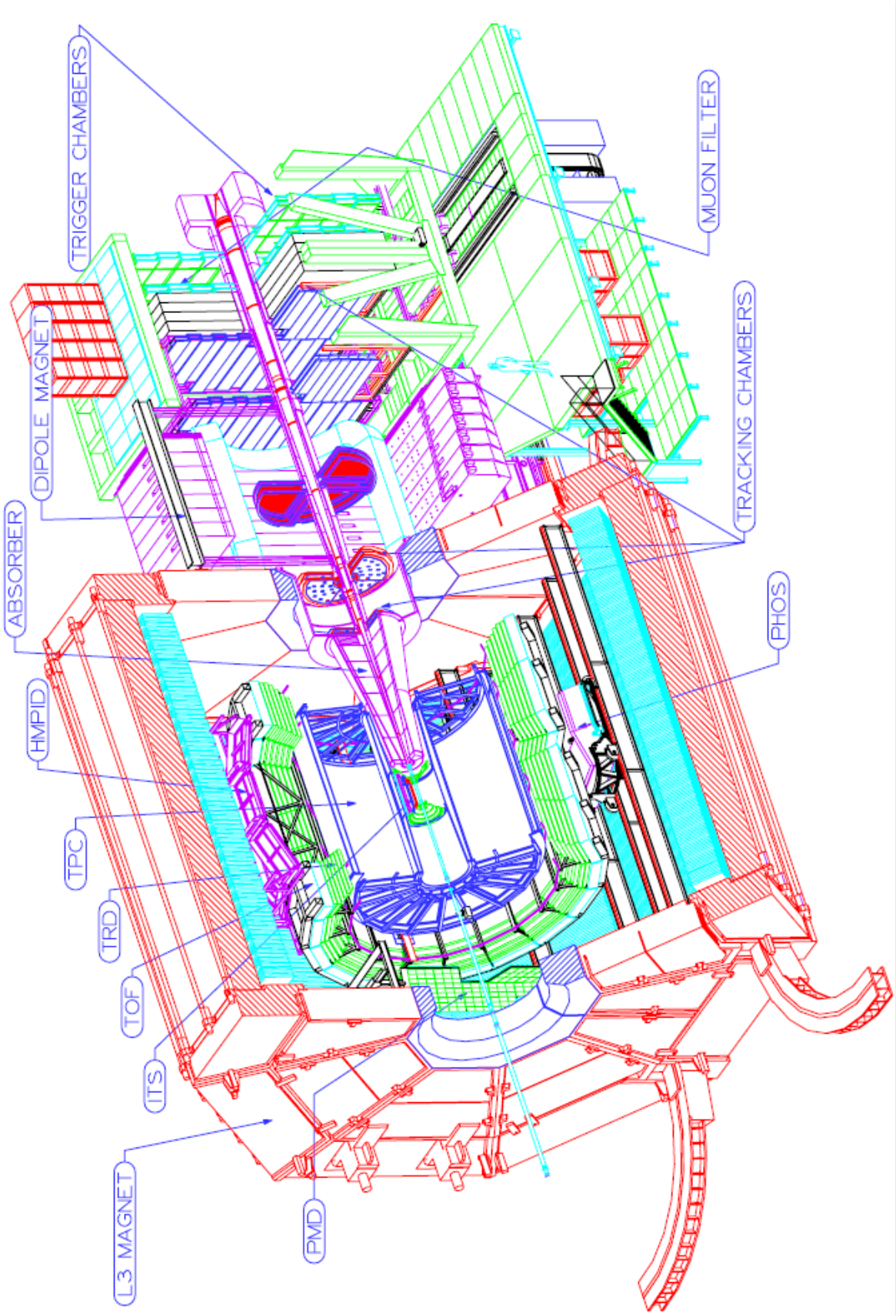

Figure 1.1: ALICE detectors

1.2.1 Tracking

Search for primary vertex is done by silicon pixel detector, ITS, which is the innermost detector of ALICE experiment. Reconstruction starts with search for clusters, set of adjacent digits, i.e signals obtained by sensitive pads in detector, in all sensitive central detectors. Tracking itself, begins in TPC, best tracker present, where overall efficiency of track reconstruction is 85% for all transverse momenta and resolution of track's energy loss is around 6%, [1]. Firstly track candidates, seeds, are found and tracking proceeds to smaller radii of TPC, where new clusters are associated to existing seeds if possible, thus refining track parameters. Second step is prolongation of tracks to ITS, when all seeds are prolongated to inner radii of TPC. Here, tracks are prolongated to primary vertex and precise ITS clusters are associated to track candidates. Also, in ITS impact parameters are calculated with respect to previously found primary vertex. To some degree, data from TRD help in improvement of momentum resolution of tracks.

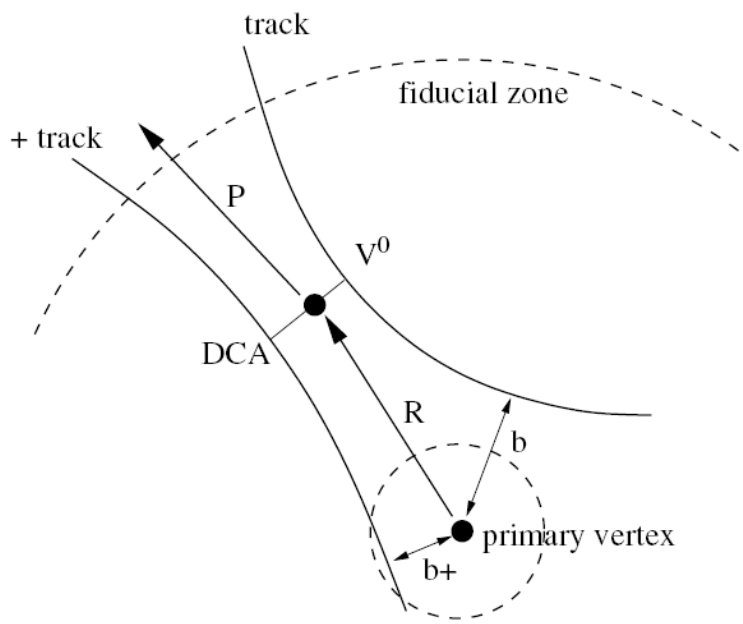

Figure 1.2: V0 reconstructed using tracks of opposite charges, with sufficient impact parameters, b, and small enough distance of closest approach

In the last step cascades, V^0's and kinks from secondary vertices are reconstructed using reconstruction algorithm in ITS and TPC. V^0 reconstruction, i.e. reconstruction of neutral particles from pair of tracks with opposite charge as depicted in Fig. 1.2, is done by selecting secondary tracks with sufficient impact parameters. Afterwards, combinations of 2 tracks of opposite charge create possible secondary vertices. These are rejected based on DCA cut placed on these two particles, and position of this closest approach. As last, momenta of V^0 is checked with respect to primary vertex.

Similarly, cascade, subsequent decays of decay particle created, reconstruction starts with search for V^0 with large impact parameter, Fig. 1.3 depicts cascade decay of Ω^- (Ξ^-) through Λ^0 as V^0. Next is selection of

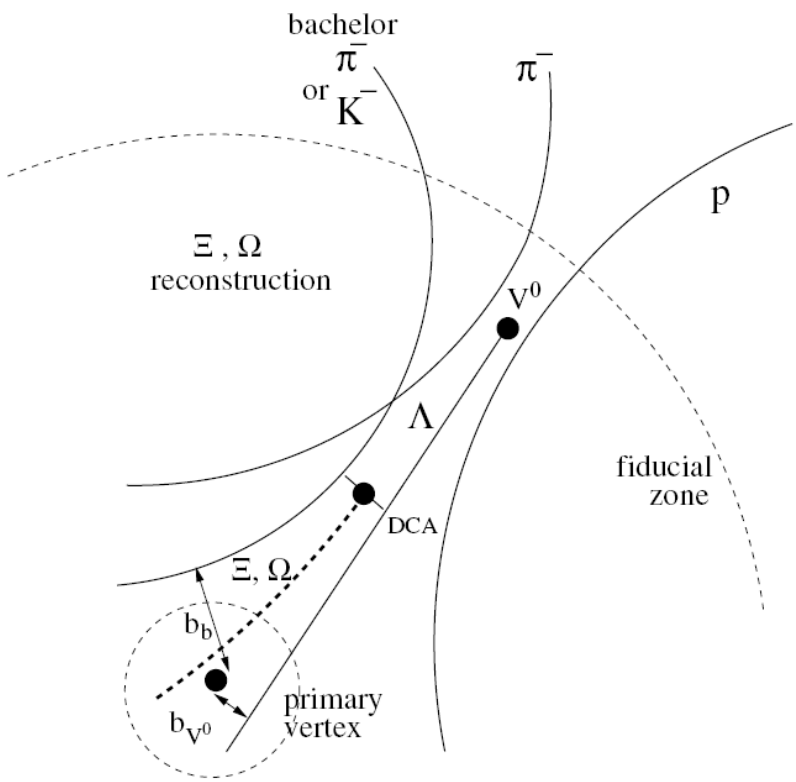

Figure 1.3: Reconstruction of cascade decay of Ω^- (Ξ^-) through Λ^0

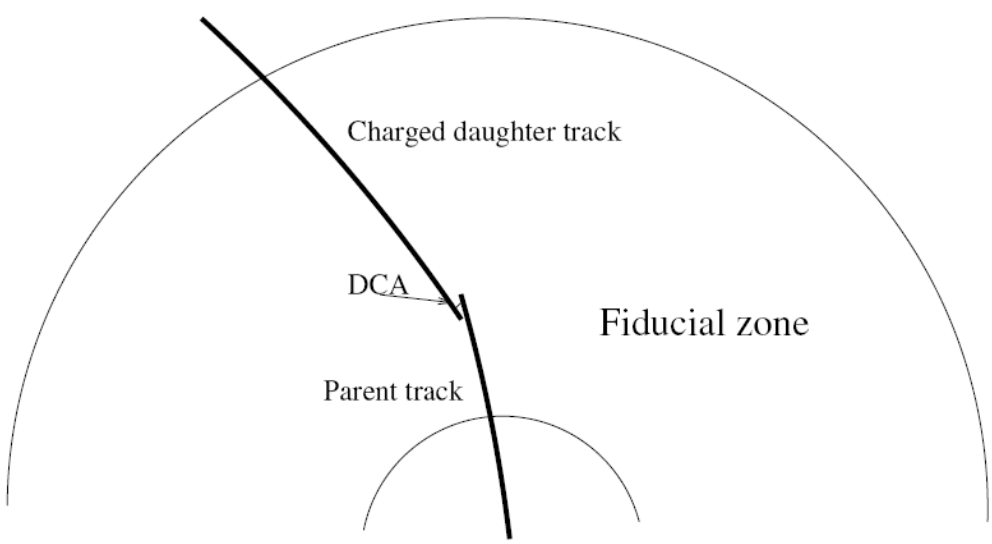

Figure 1.4: Kink, signature of 1-prong decay

secondary bachelor track candidate, with small enough DCA to calculated trajectory of V^0. Again momenta at this decay vertex is check with respect to primary vertex.

Reconstruction of kinks, Fig. 1.4, sign of 1-prong decay like $K \to \mu\nu$ or $\pi \to \mu\nu$, is done by finding 2 tracks of same charge with small DCA.

1.2.2 Particle identification

Information for particle identification (PID) of charged particles is provided by ITS, TPC, TRD, TOF and HMPID detectors.

ITS provides information in non-relativistic region . In cases of low momenta particles it is the only source of their type. In this detector energy is lost in silicon detectors.

In TPC, charged particles ionize gas and lose energy. This loss can be calculated according to Bethe-Bloch's formula.

TRD detector mainly differentiates between electrons and pions. As name signifies, it uses transition radiation for identification, similarly TOF detector utilizes time signatures matching reconstructed tracks and HMPID is detector designed to help identify hadrons with high momenta. With it's help, for electron identification efficiency of 90%, pion suppression of 100 is achieved.

Combining information from different detectors is complicated, because identification in certain region and detector may have different weight than in in other detector. For example signal for the different particle types at given momenta may be same for one detector but completely different in second detector.

ALICE should be able to identify charged particles with momenta from 0.1 GeV/c up to few GeV/c, and up to several tenths GeV/c using dE/dx information.

1.3 Reconstruction of jets

Reconstruction of jets may be much more difficult than tagging. It is so, because we do not see what really happens before hadronization, when fragmentation occurs. We don't even see all the products, because neutral particles are practically invisible for tracking. With PHOS we may be able to identify part of photons.

Photons shall be identified also in electromagnetic calorimeter, which with ALICE's tracking system shall provide excellent jet quenching measurements. It is designed to improve jet energy resolution, provide triggering of high-energy jets, improve measurement of high energy electrons and photons ... EMCal is segmented into 12288 towers, each having $\Delta\eta = 0.014$ and $\Delta\phi = 0.014$

Jet reconstruction is mostly done by measuring electromagnetic and hadronic energy deposited in calorimeters. In ALICE, hadronic energy is measured by tracking of hadronic charged particles. This is preferred method in heavy-ion collision where due to large background fluctuations tracking enables better rejection of low energy hadrons from soft background. Energy deposited in EMCal from hadronic particles is removed by association of hadronic tracks to clusters of EMCal's energy towers.

The most used algorithm to reconstruct jets is based on grouping energy towers inside a circle of given radius in coordinate system of rapidity and azimuthal angle, alternatively rapidity may be substituted by

pseudo-rapidity. Circle together with primary vertex as apex create cone, therefore cone algorithm. This was originally developed by UA1 group and simple depiction is in Fig. 1.5

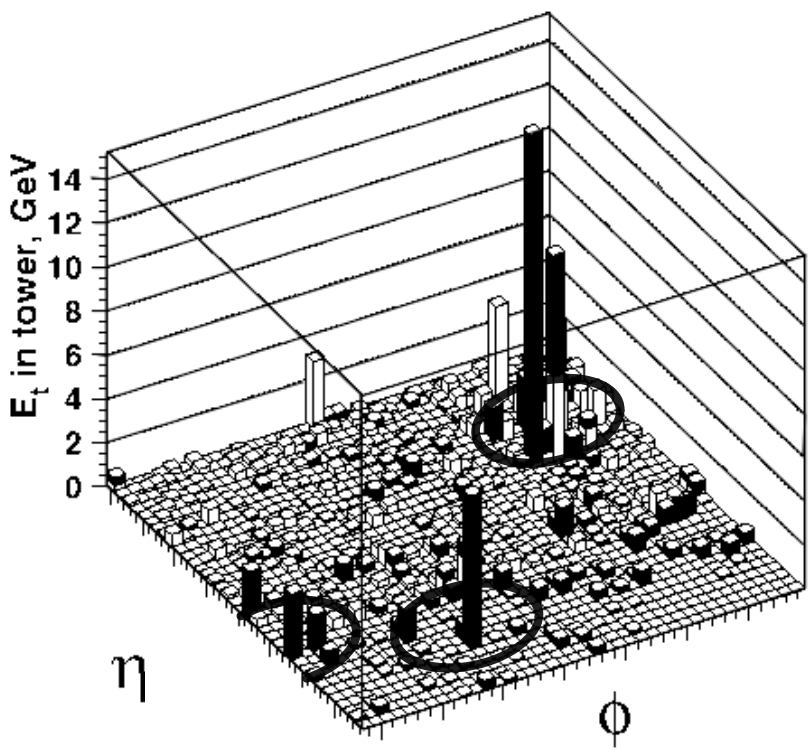

Figure 1.5: Simple depiction of grouping up energy towers inside circle within radius from seed.

1.3.1 Cone algorithm

There exist two main types of cone algorithm, seeded and seedless. Both group together all energy towers inside radius $R = \sqrt{\Delta\eta^2 + \Delta\phi^2}$ where Δx signifies distance in x-coordinate of given energy tower from center of cone. The difference between two types of cone algorithm is based on a way how to find center of cone. Seeded algorithm looks for energy tower, or energy of hadronic particles, which is greater than certain threshold. Afterwards center of cone is shifted to position of coordinates of weighted center, which is taken as new seed and process is iterated until stable position is found, i.e. until inclusion of particles at

the border of jets does not move weighted center, much. Seedless algorithm is in fact same, but in order to find center of jet-cone it iterates over all energy towers, hadronic particles' tracks, as if they were seeds. This algorithm contains one more step and that is checking if reconstructed jet-cone wasn't reconstructed in previous iteration.

In heavy-ion experiments background reduction is included. Placing cut on transverse momenta of charged tracks, $p_T \geq 2$ GeV/c , removes significant amount of background, in this case 98%. Than energy towers are sorted according to decreasing transverse energy and taking most energetic tower as a seed run cone algorithm. At the end background energy per tower is calculated from energy outside of reconstructed jets. Subtracting background energy per tower from all towers algorithm undergoes second iteration/ These steps are repeated again and again until result of one iteration isn't same or differs only a little from previous iteration.

Also cone radii differ for heavy-ion collisions. In pp collisions, radius is usually set to 0.7 or 1.0. In heavy-ion collisions this is smaller because with larger radius amount of background energy included increases, however, in this way part of jets energy is excluded from reconstructed jet.

Using seeds, cone is created around most energetic particles.

1.3.2 Other properties of cones

In jet reconstruction we may come across several problems, for example when two cones are reconstructed so they overlap, when do we merge them. If energy in overlap region is smaller than preset fraction of energy of cones, these are merged, otherwise they energy towers in this region are associated to cone whose center is closer. Overlapping cones are mainly due to fact that cone algorithm is in general not infrared safe.

Similarly due to deposition of energy from one particle to several towers, creation of cone may not be triggered, because seed won't be created. Therefore cone algorithm is generally collinearly unsafe.

Efforts are made to create SISCONE, algorithm that would overcome these hindrances.

Chapter 2

Analysis

2.1 AliRoot

In my analysis, I was working with official ALICE software, *AliRoot*. I used version v4-16-Rev00, together with *Root* v5-21-01-alice. *Pythia* implemented was v6-4-16 and detector response was done by *Geant3* version v3-1-9. Generating 202980 proton-proton collisions at 14TeV center of mass energy, with gluon radiation and 0.5T magnetic field. In every event, pair of b-quark and b-anti-quark wes created which after hadronisation underwent forced semi-electronic decay. Subsequently after simulation, these data were reconstructed.

2.2 Kinematics of jets

First of all, I tried to investigate how does daughter products of b-quark behave, at what angles with respect to momenta of mother particle do they travel, what portion of energy do they have etc. In sample of p+p collisions I simulated were altogether 404562 b-quarks hadronizing and consecutively decaying with electron as one daughter product. Kinematic distribution of these quarks is in Fig. 2.1a and Fig. 2.1c. However, I selected only b-quarks present in η region smaller than 1 and greater than -1. Distribution of these is in Fig. 2.1b and Fig.2.1d. These b-quarks have energy spectrum plotted in Fig. 2.1f. In all these figures data are normalised to 1, having on y-axes fraction of all the data.

2.2.1 Radiation from b-quark

Starting from b-quark, mainly gluon and photon emission occurs. This process has two daughters, one of which is b-quark. Momentum of daughter b-quark is changed with respect to momentum of mother b-quark, angle they contain has mean value equal to 0.014 radians. This is seen in Fig. 2.2a, while from cumulative frequency, Fig. 2.2b, we see that roughly 75% of cases has angle smaller than this mean and majority, around 93% of cases, has angle small or near 0.1. Notable is that 64% of angles is smaller than 0.001 radians

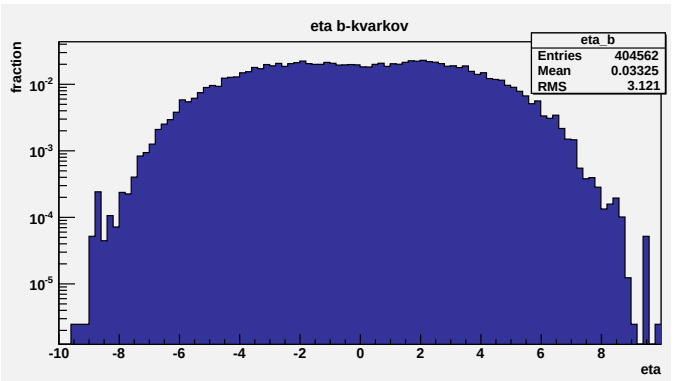

(a) eta distribution w/o selection

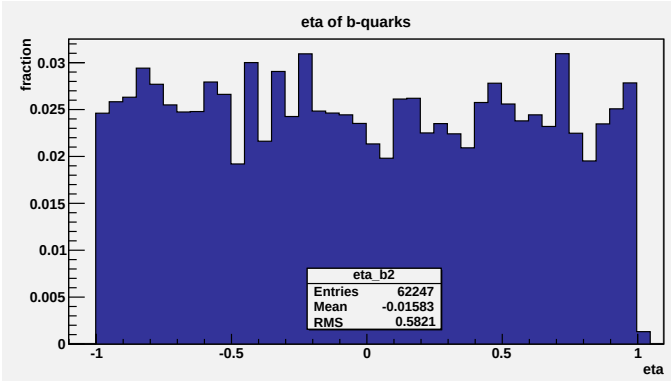

(b) eta distribution of selected

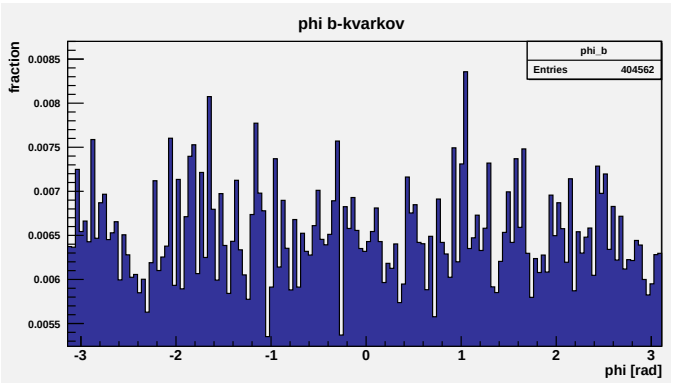

(c) phi distribution w/o selection

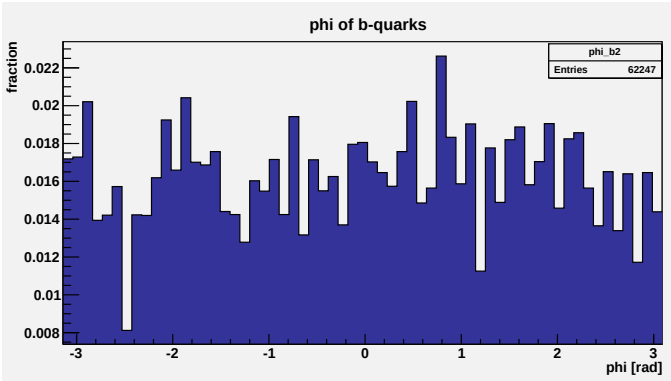

(d) eta distribution of selected

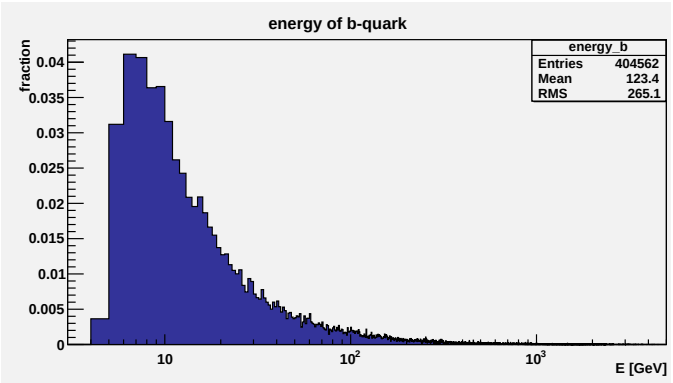

(e) Energy spectra w/o selection

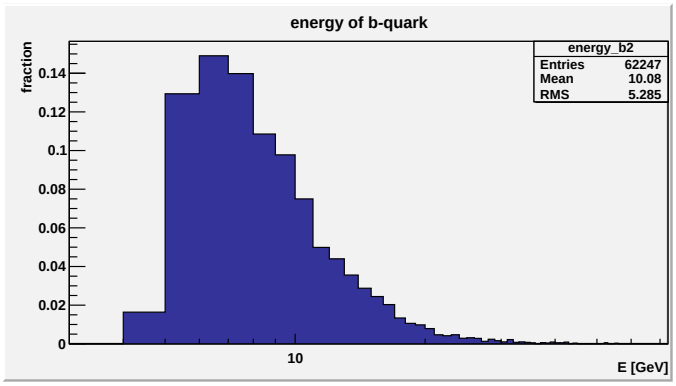

(f) Energy spectra of selected

Figure 2.1: Kinematics of produced b-quarks with and without selection of η range $\langle -1, 1 \rangle$.

From the point of view of variables η and ϕ, the distance ΔR, defined in section dealing with jet reconstruction, between the original and new b-quark is seen ,in Fig. 2.2c, to have mean value equal to 0.027. Due to η dependency of ΔR, there is still nearly 1% of angles in bin with $\Delta R \in \langle 0.25 - 0.35 \rangle$, but overally as seen in cumulative frequency distribution, Fig. 2.2d, 94% of angles is smaller or equal to 0.175.

During this process, b-quark loses part of its energy. Fraction of lost energy is depicted in Fig. 2.2f, where in majority only small fraction is lost, in more then 75% of cases is when less than 5% of energy is lost. Energy of new particle is in Fig. 2.2e, which is in fact energy lost by b-quark.

We can see that b-quark preserves its direction, with generally very small deflections in angle, and relatively small in ΔR. Also energy losses are very small.

2.2.2 b- & c-hadrons

Secondly, I looked into hadronisation of b-quarks to b-hadrons. In table Tab. 2.1 are pdg codes, names, number of cases and corresponding fractions of cases.

PDG code	Name	Abundance	Fraction of All	PDG code	Name	Abundance	Fraction of All
511	B^0	6650	10.7%	5212	Σ_b^0	281	0.5%
513	B^{*0}	17995	28.9%	5214	Σ_b^{*0}	583	0.5%
521	B^+	6380	10.3%	5222	Σ_b^+	229	0.4%
523	B^{*+}	18938	30.5%	5224	Σ_b^{*+}	743	1.2%
531	B_s^0	1815	2.9%	5232	Ξ_b^0	246	0.4%
533	B_s^{*0}	4880	7.8%	5312	$\Xi_b^{\prime -}$	2	0.0%
543	B_c^{*+}	1	0.0%	5314	Ξ_b^{*-}	99	0.2%
5112	Σ_b^-	219	0.4%	5322	$\Xi_b^{\prime 0}$	29	0.0%
5114	Σ_b^{*-}	561	0.9%	5324	Ξ_b^{*0}	14	0.0%
5122	Λ_b^0	2307	3.7%	5334	Ω_b^{*-}	19	0.0%
5132	Ξ_b^-	175	0.3%				

Table 2.1: Table of products of b-quark hadronisation.

In Fig. 2.3e is shown histogram of relative energy of b-quark to its hadronisation product. It's seen that hadrons of both greater and smaller energies are created. Mean value is 1.027, i.e. b-quarks mostly lose energy in this process, although two peaks are seen. First one at value 0.95, meaning that created hadron gains 5.3% of energy, second is at 1.05 meaning that 4.8% of b-quarks energy is lost.

The angle between b-quark and b-hadron, Fig. 2.3a, and it's cumulative frequency distribution, Fig. 2.3b, show that mean angle of hadronisation is 0.19 radians and 65% of all hadronisations have this angle smaller or equal to mean value. This mean is an order of magnitude greater than in b-quarks radiation of photons and gluons. Looking on Fig 2.3c and Fig. 2.3d we see that mean value of ΔR is 0.24 and around 68% of all cases have value of ΔR smaller or equal to this mean value.

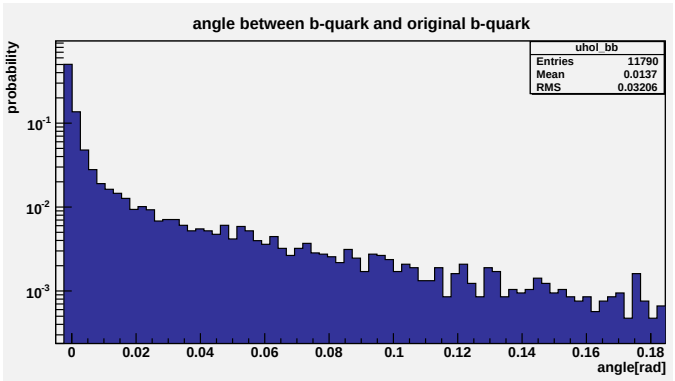

(a) b-quark's angle distribution during radiation

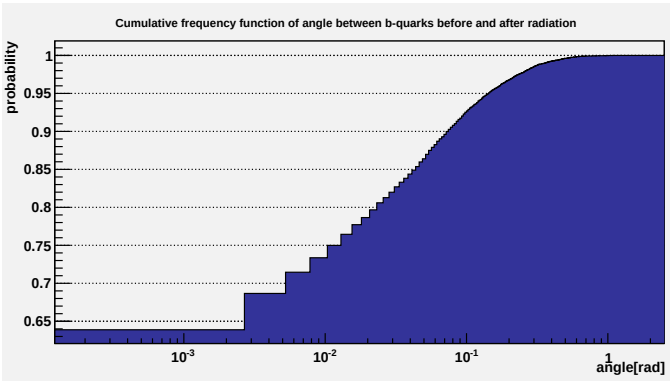

(b) b-quark's cumulative frequency distribution of angle

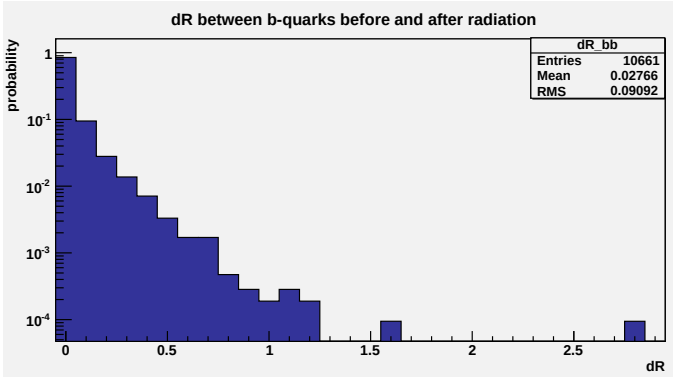

(c) ΔR between b-quarks in particle radiation

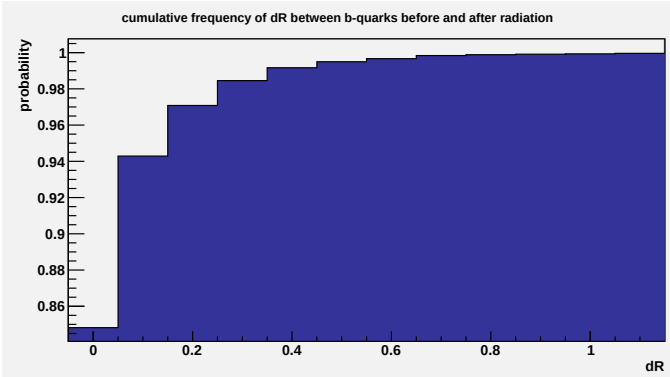

(d) cumulative frequency of ΔR between b-quarks

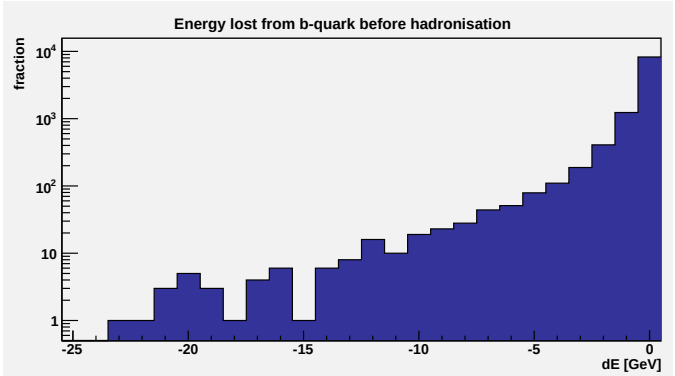

(e) Energy lost in radiation from b-quark

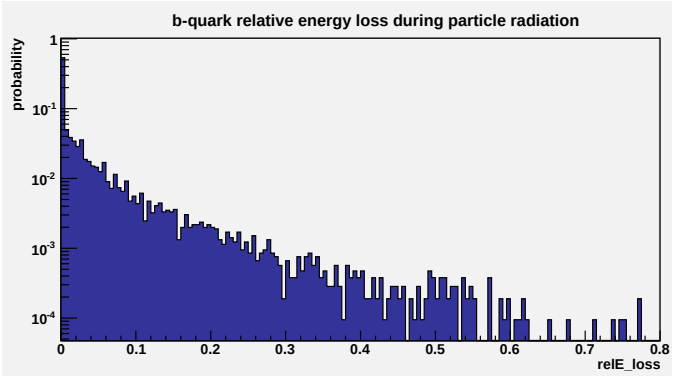

(f) Fraction of b-quark's energy lost during radiation

Figure 2.2: Radiation from b-quark.

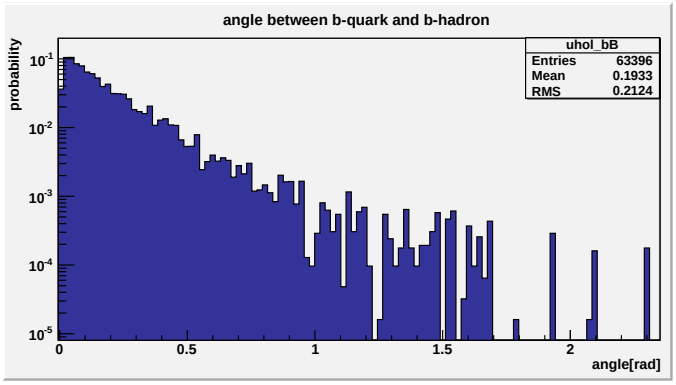

(a) Angle between b-quark and b-hadron.

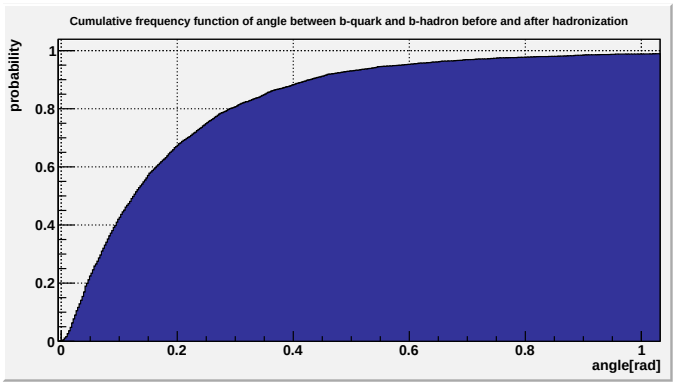

(b) Cumulative frequency of angle from Fig. 2.3a.

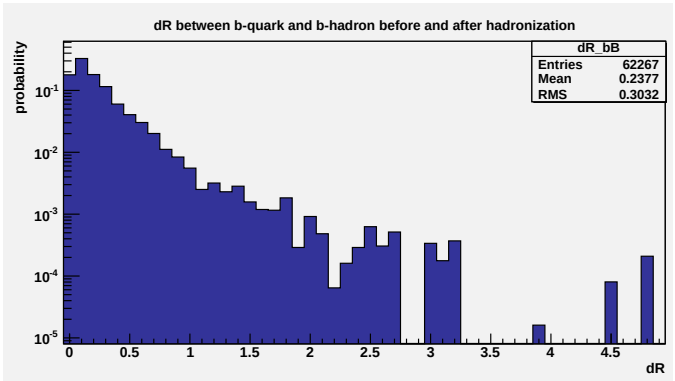

(c) ΔR between b-quark and b-hadron.

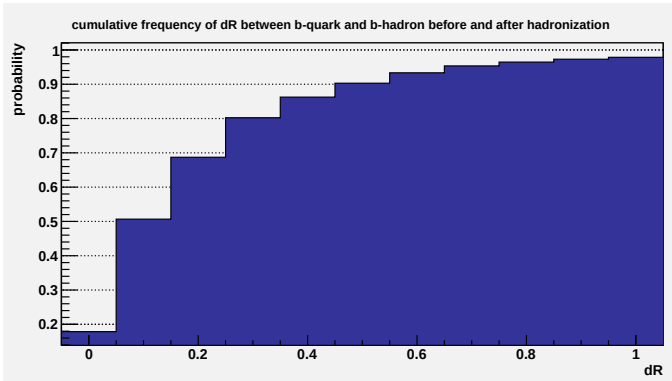

(d) Cumulative frequency of ΔR from Fig. 2.3c

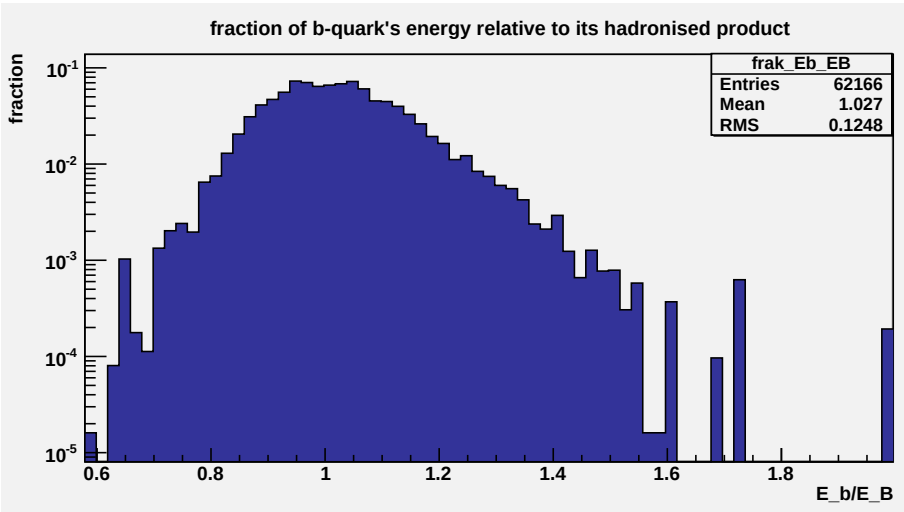

(e) Fraction of energy b-quark's energy to b-hadron's

Figure 2.3: Hadronisation of b-quark.

From table Tab. 2.2 we see that b-hadron may decay to hadron containing charm creating electron and anti-neutrino, however, it may emit also photons and pions, creating another b-hadrons.

PDG Code	Name	Abundance	Fraction of all	PDG Code	Name	Abundance	Fraction of all
decay to c-hadrons:							
11	e^-	62166	100%	12	ν_e	62166	100%
411	D^+	4776	7.7%	413	$D^*(2007)^+$	122893	20.7%
415	$D_2^*(2460)^+$	2961	4.8%	421	D^0	4861	7.8%
423	$D^*(2007)^0$	13221	21.3%	425	$D_2^*(2460)^0$	2908	4.7%
431	D_s^+	1396	2.2%	433	D_s^{*+}	3338	5.4%
435	$D_{s2}^*(2573)^+$	798	1.3%	4122	Λ_c^+	4923	3.8%
4132	Ξ_c^0	276	0.4%	4233	Ξ_c^+	289	0.005
4334	Ω_c^{*+}	19	0.0%				
decay to b-hadrons:							
22	γ	41978	94.1%				
111	π^0	864	1.9%	211	π^-	1752	3.9%
511	B^0	17995	40.3%	521	B^+	18938	42.4%
531	B_s^0	4881	10.9%	533	B_s^{*0}	1	0.0%
541	B_c^+	1	0.0%	5122	Λ_b^0	2616	5.8%
5132	Ξ_b^-	101	0.2%	5232	Ξ_b^0	43	0.0%
5332	Ω_b^-	19	0.0%				

Table 2.2: Decay products of b-hadrons, including both electronic decay to charm containing hadrons (upper part of table), where electron and its neutrino are two out of three decay products, and emission of photon or pion as one daughter particle and beauty containing hadrons as one of products (lower part of table).

In case of decays to b-hadrons, angles between mother and daughter b-hadrons is shown in Fig. 2.4a and ΔR in Fig. 2.4c. Angles and ΔR between mother b-hadron and daughter c-hadron are in Fig. 2.4b and Fig. 2.4d respectively. From these is seen that both angle and ΔR in case of pion or photon emission are very small. Mean angle is 0.007 radians and around 80% of angles are smaller than 0.01 radian.

This is similar in case of ΔR with mean value 0.0008 and majority of cases has this value smaller than 0.15. In case of beta-like decay of b-hadrons to c-hadrons, mean angle is 0.49 radians having 60% of angles smaller or equal to this mean, and with distinct peak at 0.25 radians. However, ΔR is much greater, with mean 0.6 and peak 0.3. only 45% of cases had ΔR smaller than 0.5, with lower quartile at 0.25.

For fraction of lost energy in emission, mean value is 0.012 and not exceeding 5.5%, therefore overally having little effect. This is seen in Fig. 2.5a. Mean value of lost energy is 0.007 GeV. In case of decay to charmed particles, Fig. 2.5b, relative energy loss is significant and having mean value at 0.495 and peak located at 0.55.

To make it clear, mean value of angle between c-hadrons, in emission, is 0.04 radians, as seen in

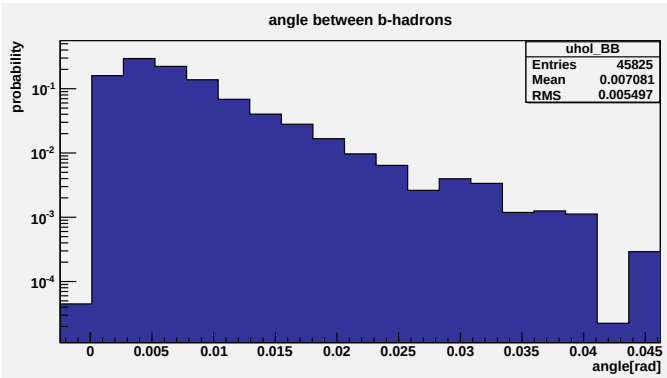

(a) Angle between b-hadrons

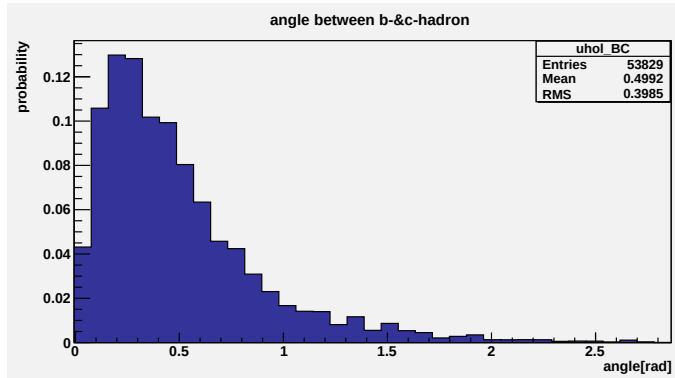

(b) Angle between b-&c-hadron

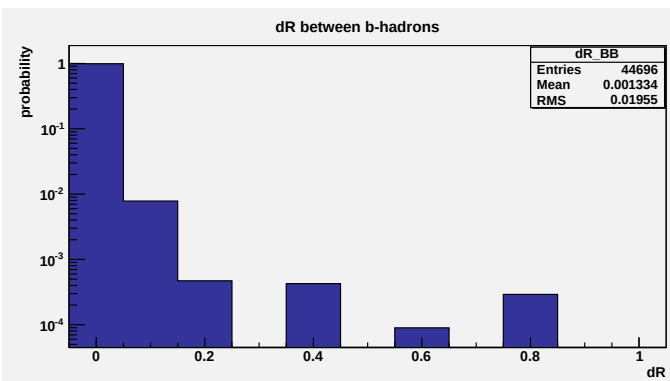

(c) ΔR between b-hadrons

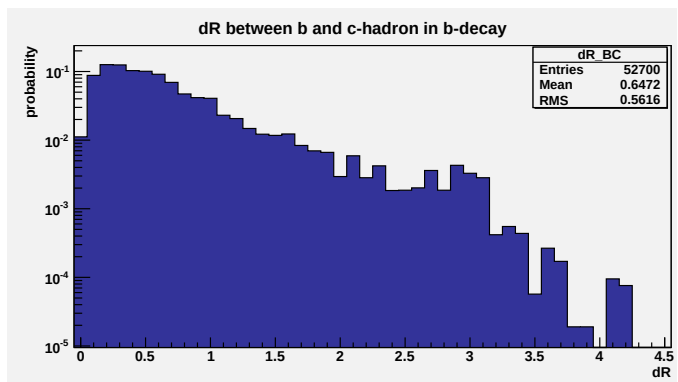

(d) ΔR between b-&c-hadron

Figure 2.4: b-hadron emission and decay geometry properties.

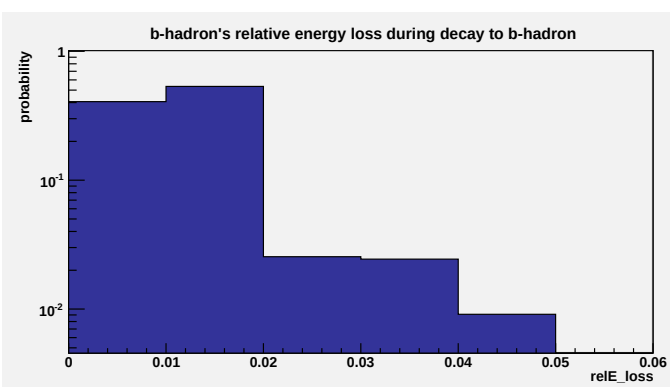

(a) Fraction of lost energy in emission

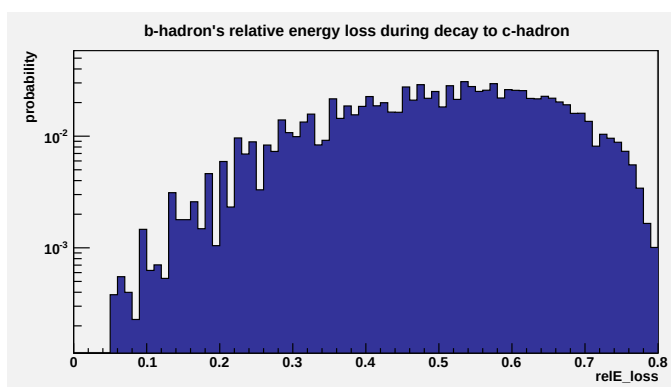

(b) Fraction of lost energy in decay to charm

Figure 2.5: b-hadron emission and decay energy properties

PDG Code	Name	Abundance	Fraction of all	PDG Code	Name	Abundance	Fraction of all
decay to charmless particles:							
11	e	52107	99.9%	13	μ	36	0.1%
130	K^0_L	8896	17.1%	310	K^0_S	8714	16.7%
311	K^0	292	0.6%	321	K^+	27280	52.3%
3112	Σ^-	25	0.0%	3122	Λ	2436	4.7%
3212	Σ^0	655	1.3%				
decay to at least one c-hadron:							
22	γ	10934	21.0%				
411	D^+	6013	11.5%	413	$D^*(2010)^+$	1277	2.4%
421	D^0	26708	51.2%	423	$D^*(2007)^0$	1319	2.5%
431	D^+_s	3338	6.4%	4332	Ω^0_c	19	0.0%
111	π^0	31705	-	211	π^+	38059	-
2112	n	1163	-	2122	p	636	-

Table 2.3: Decay products of c-hadrons, including both leptonic decay (upper part of table) and emission with charm containing hadrons as one of products (middle part of table) and particles belonging to either group (bottom part of table).

Fig. 2.6a, an order of magnitude greater than in b-hadron emission. 72% of cases have angle smaller than this mean, and to 0.08 radians corresponds cumulative frequency of 85%.

In Fig. 2.6b we see, that mean value of ΔR is 0.05, significantly greater than in case of emission from b-hadrons. 72% of cases have ΔR smaller than this mean, while 95% of data have ΔR smaller than 0.25.

From relative energy loss in this type of process, i.e. where both mother and one of daughter particles is contains charm, we see that up to 40% of energy is lost, carried away by charmless particle, while mean is at 10.1% and we observe peak at 6.5% in Fig. 2.6c. This is significantly higher than in case of similar processes with b-hadrons.

Daughter products of charm-containing particles is in table Tab. 2.3, with both decays of both types, lepton producing and c-hadron producing.

Comparing both electronic decays of b-hadrons and c-hadrons, for angles at which lepton flies with respect to original hadron, Fig. 2.7a, we see that blue line, standing for electrons from b-hadrons, has peak slightly shifted to 0.35 from red line 0.30 radians, original hadron was c-hadron. More significant is difference of mean value of 0.1 radian for b-hadron's decays equal to 0.81 and and c-hadron's decay of 0.71 radians. Statistical Kolmogorov test done in *Root* on these two samples proves that these are from same distribution. Therefore, in Fig. 2.7b we see only small difference in these cumulative frequency distributions, caused by shift in the mean and generally shallower distribution of b-hadron's decays.

From ΔR distributions and cumulative frequency distributions, Fig. 2.7c and Fig. 2.7d respectively, we again see that they are nearly same, having maxima at 0.35 for c-hadron's decay and 0.45 for b-hadron's

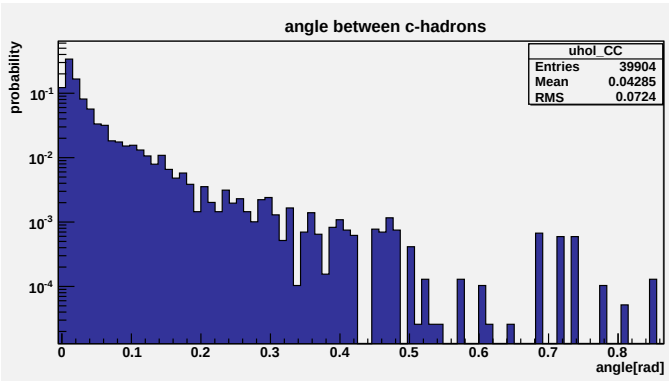

(a) Angle between c-hadrons.

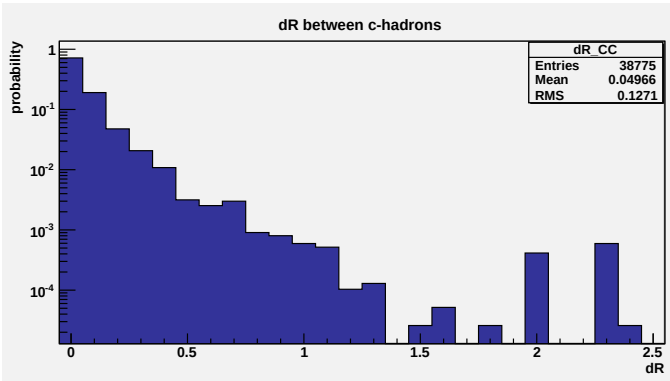

(b) ΔR between c-hadrons.

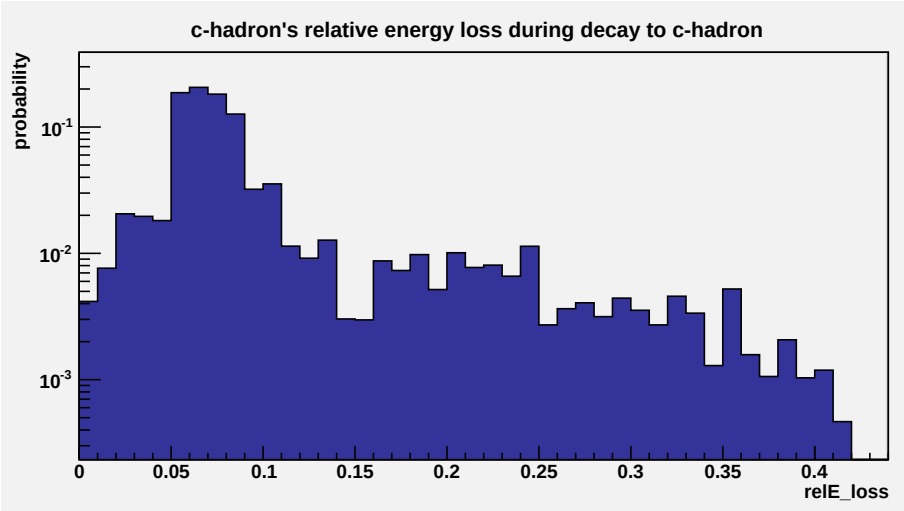

(c) Fraction of energy lost by c-hadrons.

Figure 2.6: Process with c-hadron mother and daughter particle.

decay. Mean values are at 0.95 and 1.05 with approximately 65% and 60% of ΔR having smaller value respectively. Curve corresponding to b-hadron's decay ,blue curve, becomes dominant at 0.4. At 0.5, 40% of all cases of decays from c-hadrons has ΔR smaller than this value, for b-hadron's decay this is 10% less.

From point of view of transfered energy from hadron to decay lepton, Fig. 2.7e, it's seen that spectra resembles that of β-decay. Again, in this case mean value of fraction of lepton to hadron is greater for b-hadron's decay, it's 0.26, and for c-hadron's decay, 0.22. Most probable fractions are 0.2 and 0.125 for b-hadron's and c-hadron's decay respectively, while b-hadron's decay becomes more probable than c-hadron's decay from energy fraction of 0.16.

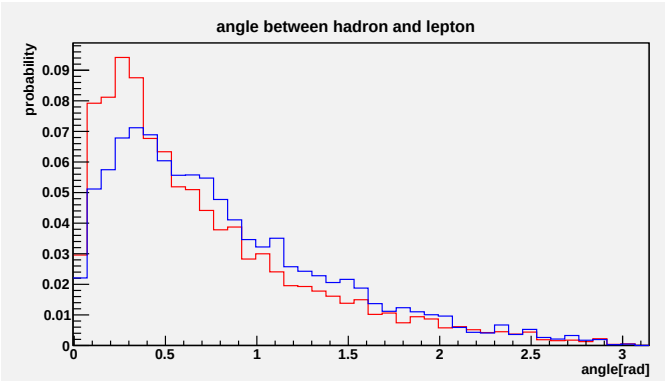

(a) Angle between hadron and lepton.

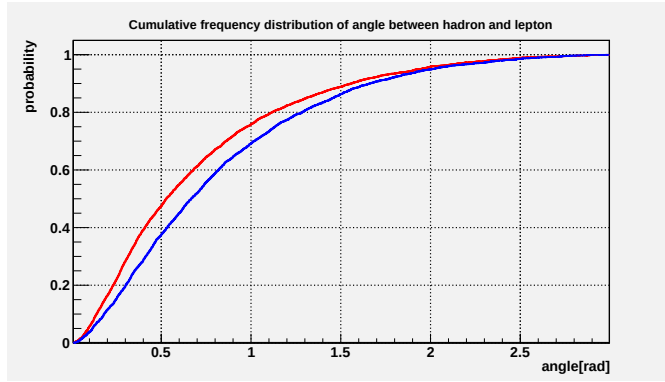

(b) Cumulative frequency of angle between hadron and lepton.

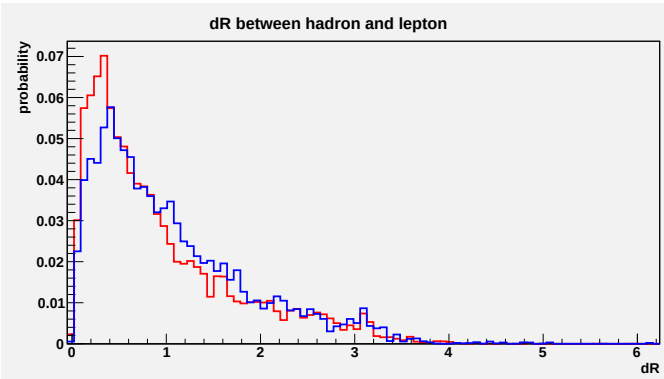

(c) ΔR between hadron and lepton.

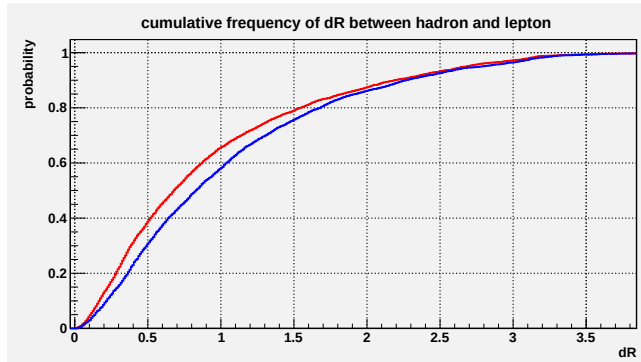

(d) Cumulative frequency of ΔR from Fig. 2.7c.

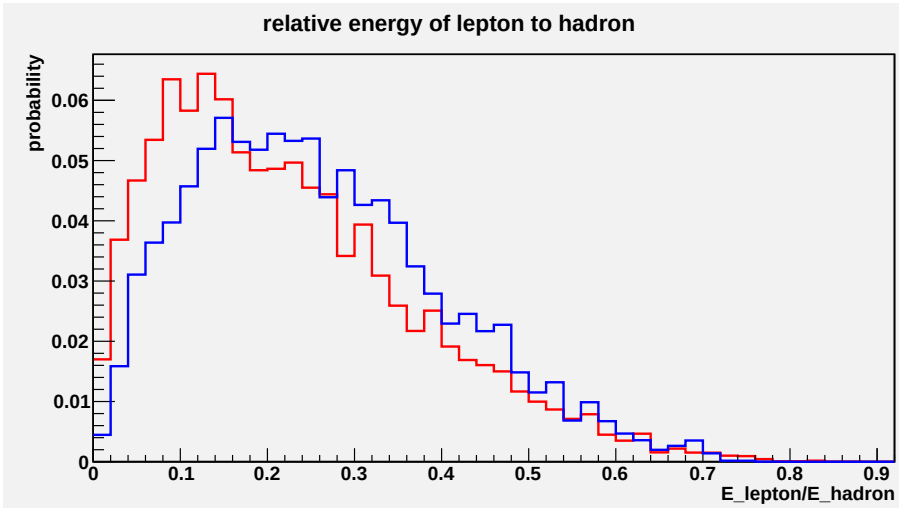

(e) Fraction of hadrons energy carried by lepton.

Figure 2.7: Red - decay of c-hadrons, Blue - decay of b-hadrons.

2.3 Track reconstruction

Concerning track reconstruction, first of all, compared number of tracks reconstructed in each event, and reconstructed after TPC and ITS refits, or both of them, which is seen in Fig. 2.8a, Fig. 2.8b, Fig. 2.8c and Fig. 2.8d respectively.

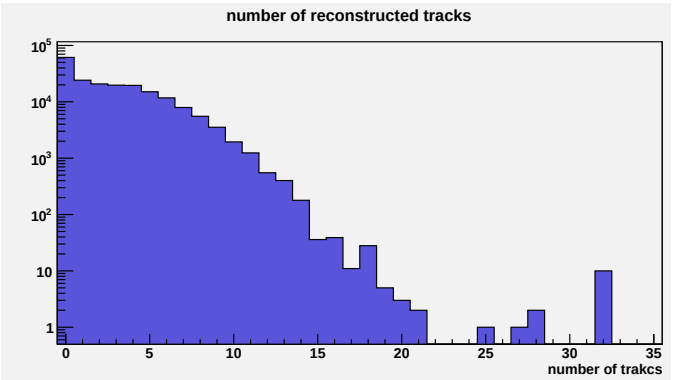

(a) Number of tracks in event.

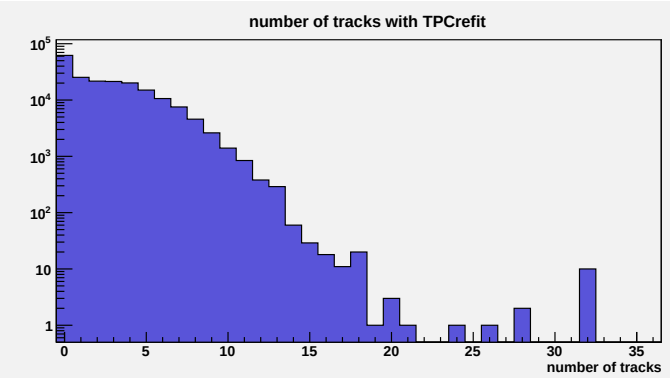

(b) Number of tracks in event after TPCrefit.

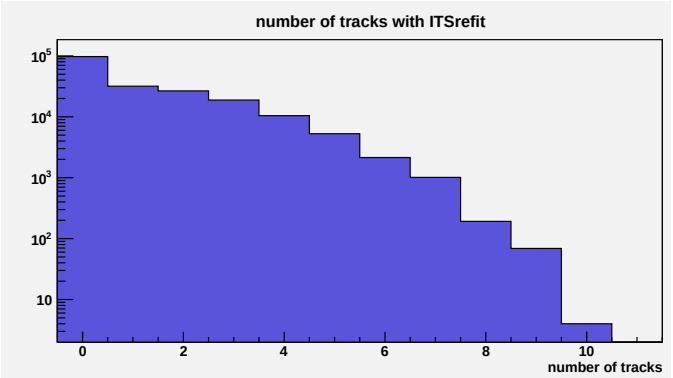

(c) Number of tracks in event after ITSrefit.

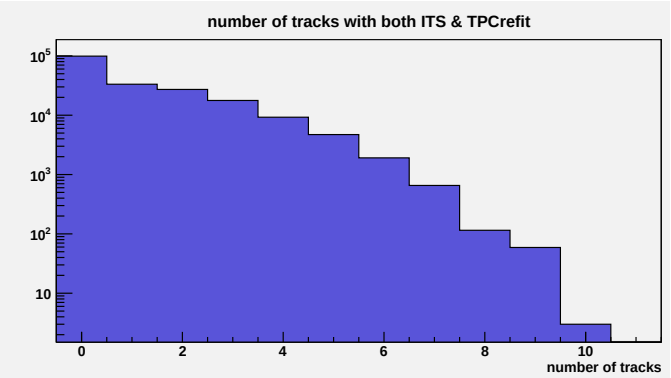

(d) Number of tracks in event after ITS&TPCrefit.

Figure 2.8: Number of reconstructed tracks in event.

From total of 221888 tracks in 196580 events, having generally 1.12 track reconstructed, 55.4% passed ITS refit. On the other hand, 71.7% passed TPC refit. Overally, 54.8% passed both TPC and ITS refits, to ensure quality of reconstructed tracks.

Track tagging itself is based on PID-probability distribution calculated by AliRoot from detector response. This probability distribution is for electrons, muons, pions, kaons and protons. Track is tagged as particle of given type, if its PID-probability is greater than probability of any other particle.

Observing eta distribution of all tracks, Fig. 2.9a, and of muons and electrons, Fig. 2.9b, we see that reconstructed tracks are indeed in η range from -1 to 1. Comparing distributions for different particle types, we see no difference.

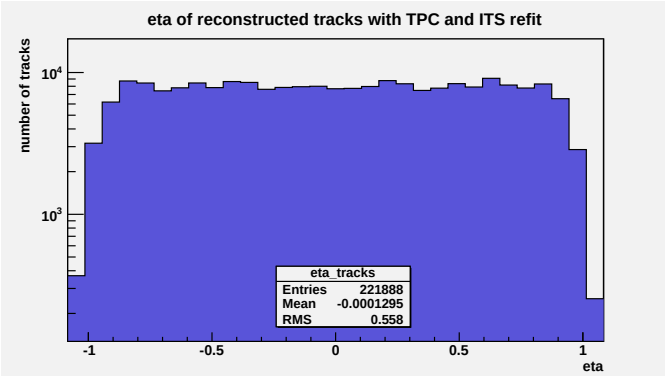

(a) Eta distribution of tracks.

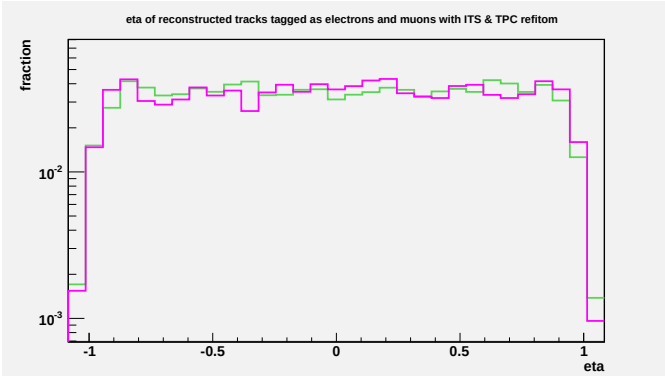

(b) Eta distribution of tracks. Green are tagged as electrons, pink as muons

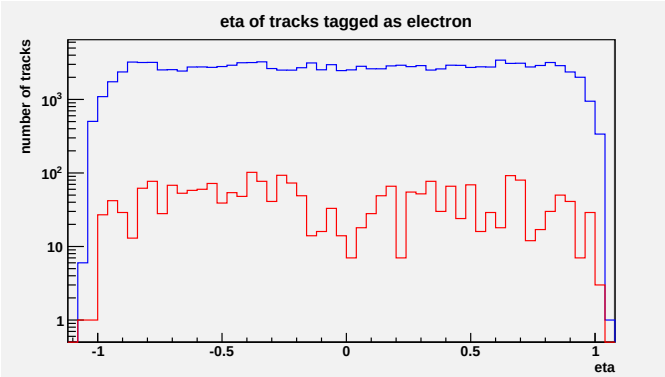

(c) Eta distribution of reconstructed particles tagged as electrons.

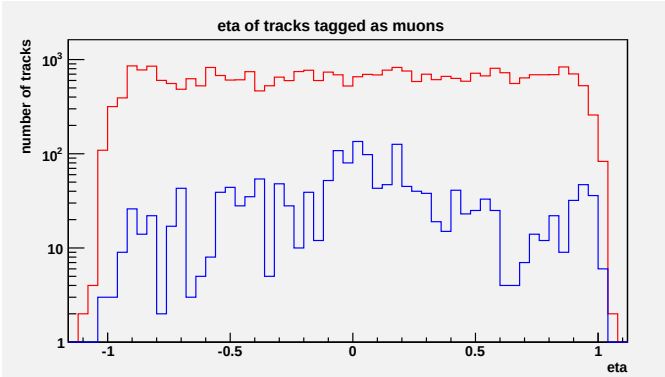

(d) Eta distribution of reconstructed particles tagged as muons.

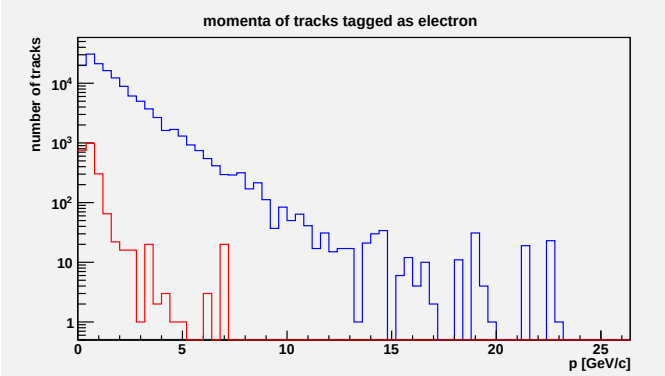

(e) Momenta distribution of reconstructed particles tagged as electrons.

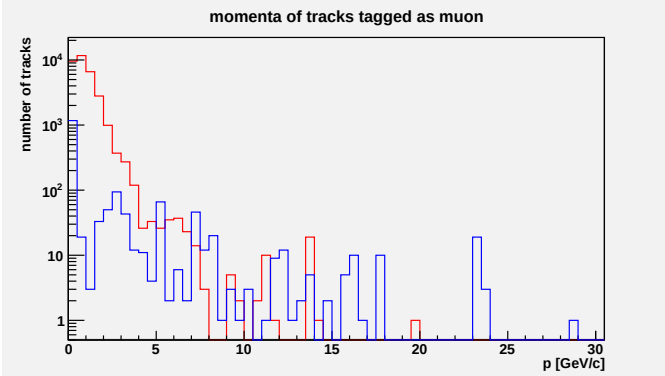

(f) Momenta distribution of reconstructed particles tagged as muons.

Figure 2.9: Properties of reconstructed tracks. In Fig 2.9c - Fig. 2.9f, red represents mistagged and blue correctly tagged tracks of given type.

In simulated sample, AliRoot reconstructed 138238 tracks subsequently tagged as electrons and 34338 as muons. In Fig. 2.9c and Fig. 2.9e, where eta and momentum distributions of correctly and incorrectly tagged electrons are shown, 98.4% of tracks tagged as electrons was correct, we see that eta distribution is similar in both cases and higher the momenta, better tagging efficiency.

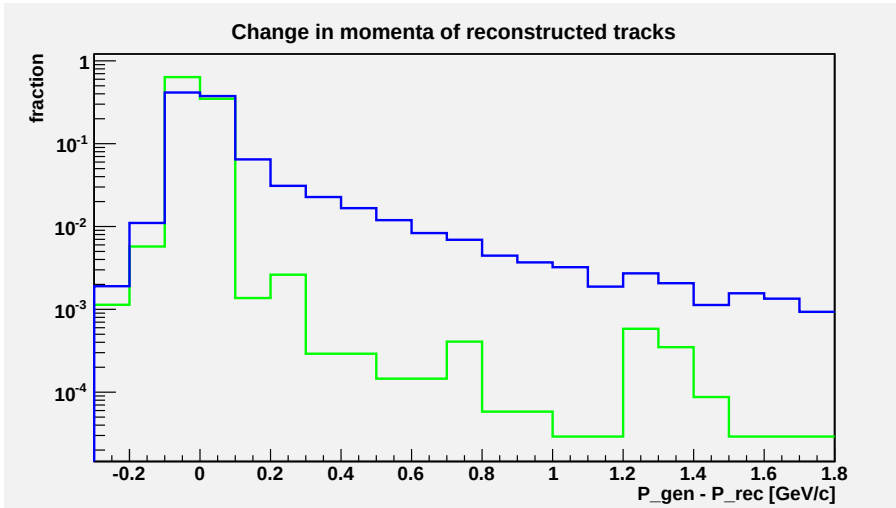

(a) Momentum loss in reconstruction of tracks.

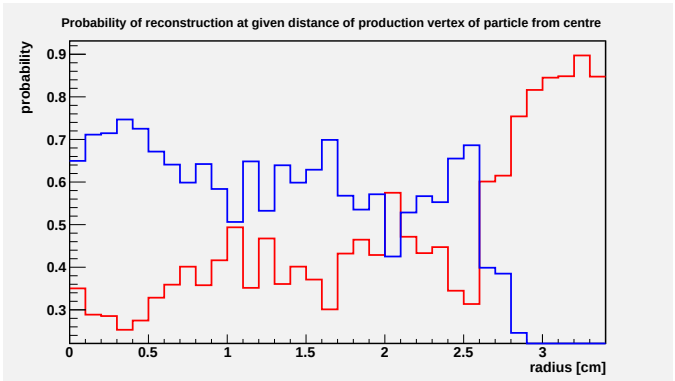

(b) Probability of particle's reconstruction w.r.t. displacement of production vertex from z-axis.

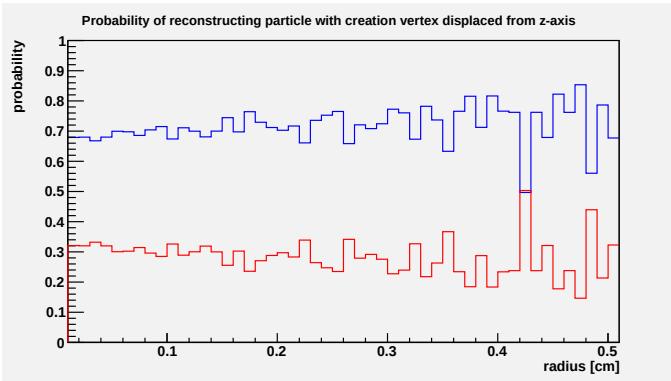

(c) Probability of particle's reconstruction w.r.t. displacement of production vertex from z-axis.

Figure 2.10: Properties of reconstructed tracks II. In Fig. 2.10a, blue stands for electrons and green for muons, in Fig. 2.10b and Fig/ 2.10c blue is for reconstructed particle, red for others.

In case of muons, Fig. 2.9d and Fig 2.9f, with efficiency of tagging equal to 4.9% , it's obvious that mistagging occurs mainly at lower momenta range, from momenta greater than 7 GeV/c, correctly tagged muons start to dominate, while at 10 GeV/c, incorrectly tagged muons occurs only exceptionally.

In Fig. 2.10a we see that momenta lost due to reconstruction are small. For muons, mean value of lost is -2 MeV/c, meaning that on average muon tracks is reconstructed with greater than simulated by 2 MeV/c. In case of electrons, tracks due to reconstruction process lose 0.1 GeV/c.

In simulation, when charged particle was created with distance of production vertex to z-axis in with η smaller than 2, it's probability of reconstruction is shown in Fig 2.10b. Reconstructed particles are mainly those, created close to z-axis as seen in Fig. 2.10c.

2.4 Reconstructed jets

In jet reconstruction, I used AliRoot's implemented UA1 cone making algorithm, with default setting for bins. As a minimum transverse energy of reconstructed jets, I used 3 GeV, 5 GeV and 10 GeV cones. I used cone of radius 1. As for seed tower, it's transverse energy was 0, 0.5 or 1 GeV. In all cases, η of jets was in interval $\langle -0.5, 0.5\rangle$, as seen in Fig. 2.11a. Just for reference, ΔR for b-quarks in event is in Fig. 2.11b, normalized to 1.

In all cases, I will look how certain property changes with increasing minimum energy of jet and increasing seed energy. For example, in case of number of jets in event, Fig. 2.13a corresponds to increasing energy of cone and Fig. 2.13b to increasing seed energy. It is seen that there are significant changes in first case, but nearly no in second. To be noted, there are 7436 jets with energy in $\langle 3, 5\rangle$ GeV with seed 0.5 GeV and 4220 jets with energy in $\langle 5, 10\rangle$ GeV and same seed. On the other hand, there are only 68 jets with energy 5 GeV and seed in $\langle 0.5, 1.0\rangle$ GeV.

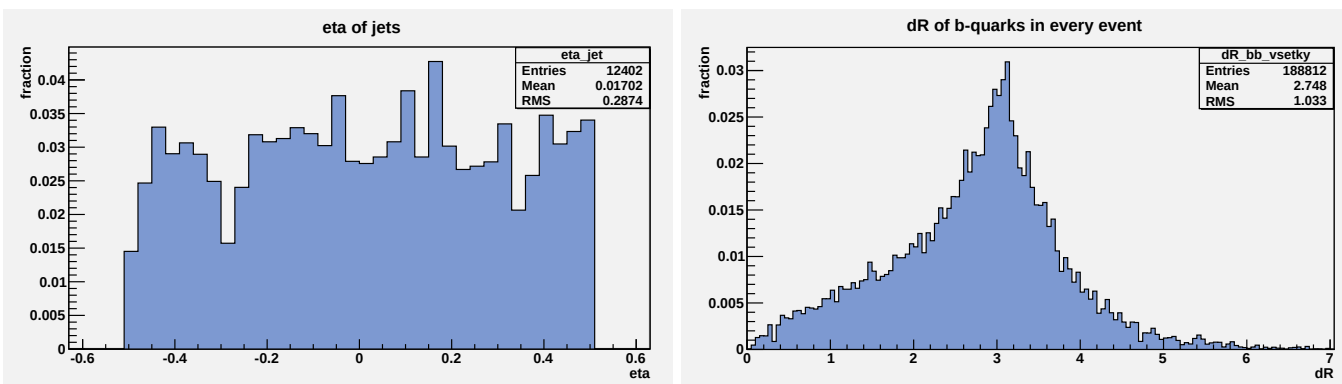

(a) Eta distribution of jets.

(b) Distribution of ΔR between b-bbar pairs in event.

Figure 2.11: Distributions.

In previous section I discussed distance in η-ϕ coordinate system between different particles, now I am going to do similar thing but with jets.

First of all, what that distance is between jet-axis and b-quark. In Fig. 2.14a, showing distribution of ΔR between b-quark and jet for cones with energies greater than 3 GeV, red line, 5 GeV, blue line, and 10 GeV, green line. Peak values for these distributions are at 0.25, 0.13 and 0.05 respectively, signifying that with greater cone energy threshold jet-axis is closer to b-quark. In these figures, second peak is seen at roughly 3.14, considering that distribution in Fig. 2.11b shows peak at this value, we can assume that this second

Colour	E_{cone}^{min} [GeV]	$E_{seed}^{threshold}$ [GeV]
red	3.0	0.5
pink	5.0	0.0
blue	5.0	0.5
black	5.0	1.0
green	10.0	0.5

Figure 2.12: Table of colours, and energy values associated with it, used in histograms.

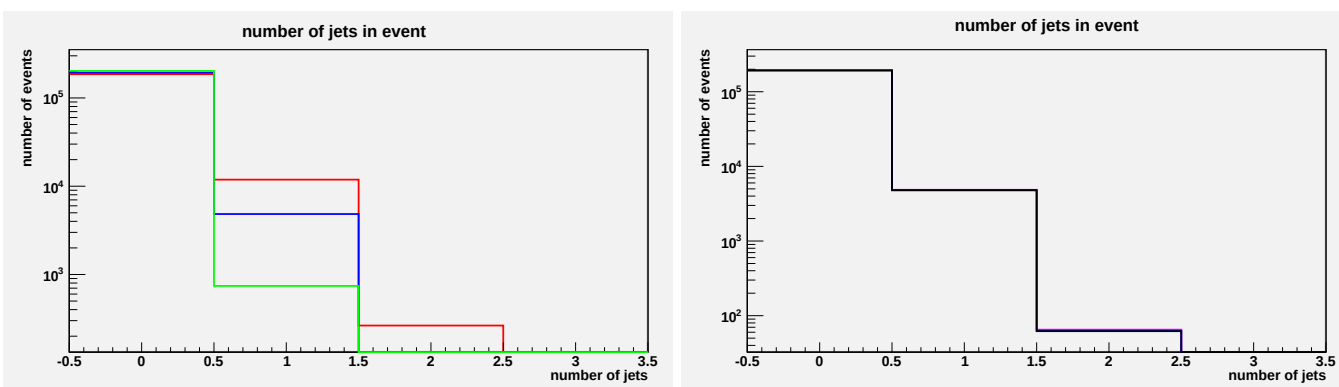

(a) Jets with same seed energy.

(b) Jets with same cone energy threshold.

Figure 2.13: Number of jets in event.

peak is clearly associated to b-quarks, created in pair with jet producing b-quark. Colours and energy values associated with it, are summed in table Tab. 2.4.

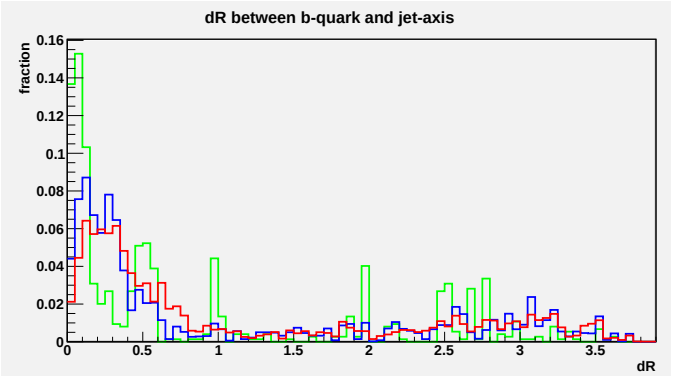

(a) ΔR distribution between b-quark and jet with increasing cone energy.

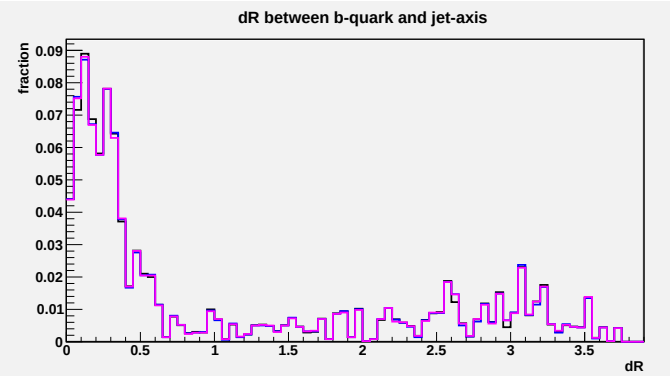

(b) ΔR distribution between b-quark and jet with increasing seed energy.

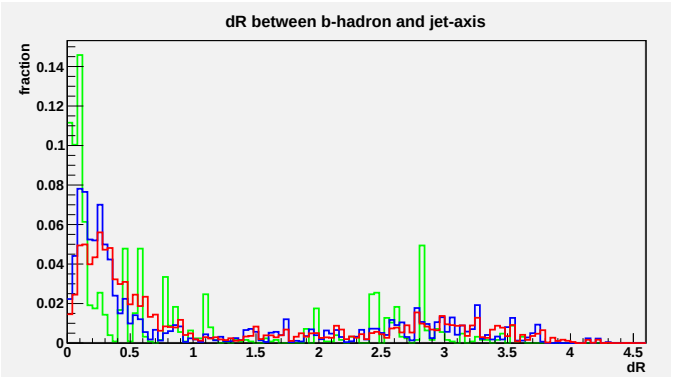

(c) ΔR distribution between b-hadron and jet with increasing cone energy.

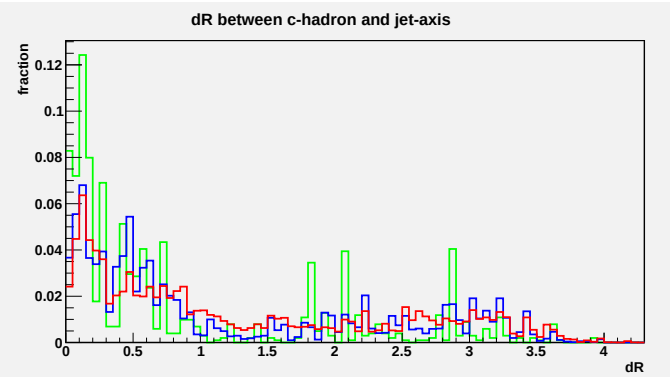

(d) ΔR distribution between c-hadron and jet with increasing cone energy.

Figure 2.14: ΔR distribution between jet and different particles.

In Fig. 2.14b is seen distribution of ΔR between b-quark and jet, for increasing seed energy, 0 GeV is pink line, 0.5 GeV is blue again, and 1.0 GeV is black, for cone energy 3 GeV. It is obvious that there are only small insignificant differences in these distributions.

Similar distributions are in Fig 2.14c and Fig. 2.14d, showing distributions of ΔR between jet-axis and b-hadron and c-hadron originating from b-quark respectively, for increasing cone energies as in previous case.

For case of b-hadrons, we see peaks at 0.2, 3 GeV cone threshold, 0.15, for 5 GeV, and 0.06 for 10 GeV threshold. Compared to this respective peak values for c-hadron case are 0.125, 0.1 and 0.05, seeing that c-hadrons are in general closer to jet-axis than b-hadrons.

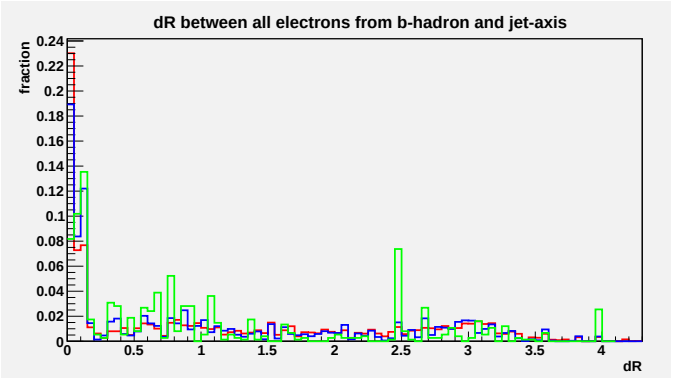

(a) ΔR distribution between electron from b-hadron and jet with increasing cone energy.

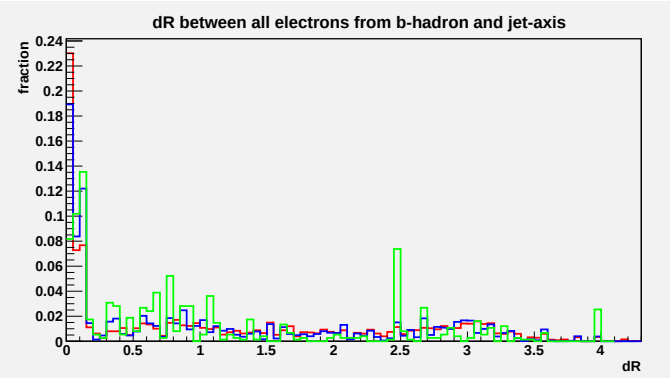

(b) ΔR distribution between electron from b-hadron and jet with increasing seed energy.

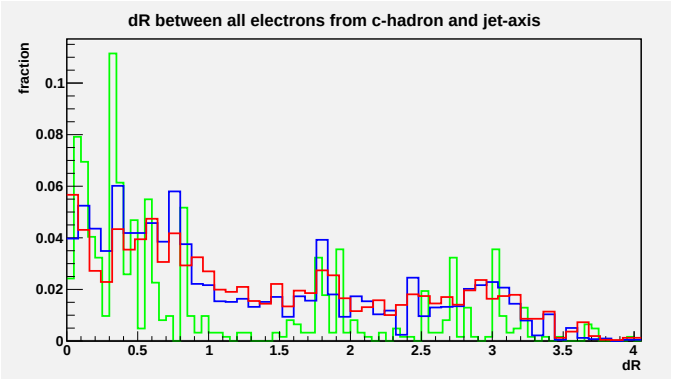

(c) ΔR distribution between electron from c-hadron and jet with increasing cone energy.

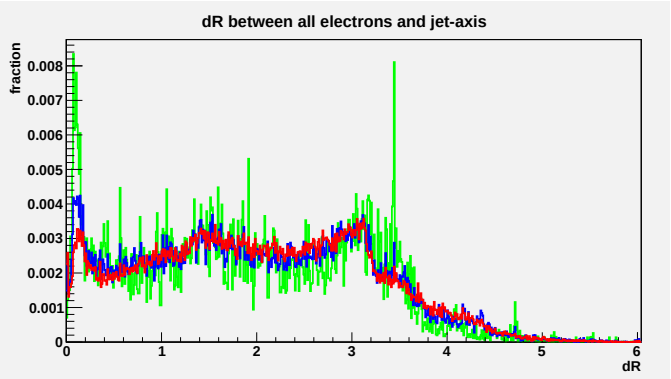

(d) ΔR distribution between all electrons and jet with increasing cone energy.

Figure 2.15: ΔR distribution between jet and electrons from different particles.

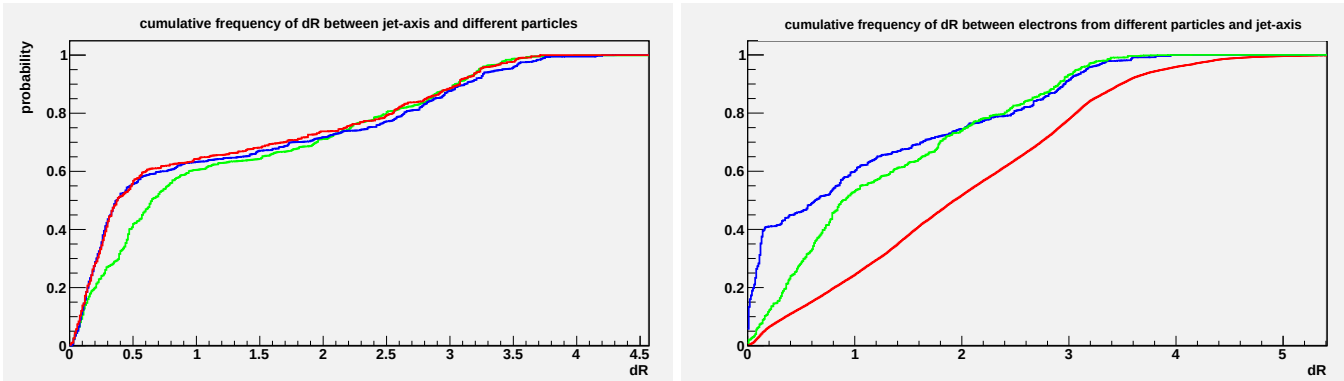

(a) Cumulative frequency distribution of ΔR between b-quark(red), b-hadron(blue) or c-hadron(green) and jet.

(b) Cumulative frequency distribution of ΔR between all electrons(red), electrons from b-hadrons(blue) or from c-hadrons(green) and jet.

Figure 2.16: Cumulative frequency distributions of ΔR and different particle types for seed energy 0.5 GeV and cone threshold 5 GeV.

Comparing cumulative frequencies of all three particle types, red for b-quarks, blue for b-hadrons and green for c-hadrons, in Fig. 2.16a we see that both b-quarks and b-hadrons have nearly same ΔR distribution, while c-hadrons are have higher probability of appearance at higher values.

However, we do not observe these hadrons directly, therefore more meaningful observation is ΔR of electrons from jet-axis.

First of all is case of electrons from b-hadrons. In figures Fig. 2.15a and Fig. 2.15b are depicted electron distributions for same seed energy of 0.5 GeV and increasing cone energy threshold in first case, and same cone energy threshold and increasing seed energy in second case.

From Fig. 2.15a we see that with increasing energy peak of ΔR between electron from b-hadron and jet is moving from 0, 3 GeV cone threshold represented by red line, to 0.1 for 10 GeV cone threshold represented by green line. In Fig. 2.15b we see that for different seeds these distributions are practically same.

Secondly, ΔR between electrons from c-hadrons and jets, Fig 2.15c, where red is 3 GeV cone, blue is 5 GeV cone and green is 10 GeV cone threshold, these distributions are nearly same with peak at 0.15-0.2. Difference for green line is because number of reconstructed cones is much smaller, therefore not having as good statistics.

Compared to ΔR between all electrons and jet, Fig. 2.15d, we see one distinct peak at around 0.11 and smaller peak at 0.01-0.02. This smaller peak is due to electrons from b-hadrons. Another bumps are at 3.14 and 1.56.

Cumulative frequency distributions of these distributions is summed up in Fig. 2.16b. here we clearly see that appearance of electrons from b-hadrons, blue line, is much higher for smaller values of ΔR in comparison to electrons from c-hadrons, green line. More than 40% of electrons from b-hadrons is present inside of subcone of radius 0.2, while for same subcone, there there is only 10% probability of electron

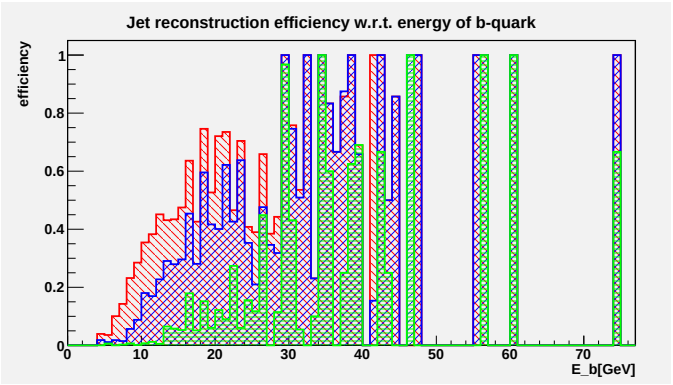

(a) Efficiency of reconstruction w.r.t. E of b-quark.

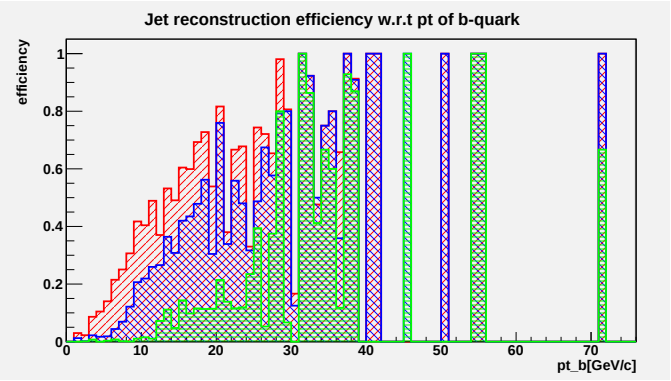

(b) Efficiency of reconstruction w.r.t. p_T of b-quark.

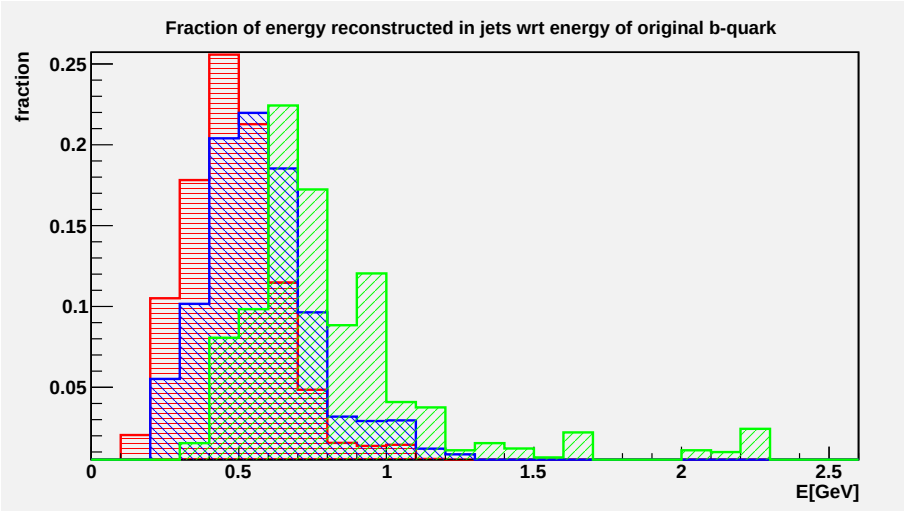

(c) Energy fraction of b-quark reconstructed in jet.

Figure 2.17: Jet reconstuction efficiencies.

from c-hadron being present. For reference, red line represents cumulative frequency distribution of all the electrons present in the event.

Considering reconstruction efficiencies, these are shown in Fig. 2.17a and Fig. 2.17b. It is seen that in both figures all curves have same shape, but are shifted due to different energy thresholds set on reconstructed cones. Again red stands for 3 GeV, blue for 5 GeV and green for 10 GeV. Due to the fact that in different energy bins are different numbers of produced b-quarks, and with increasing energy this number decreases, efficiencies for greater energies do not have same value as those at lower energies.

Lastly, in Fig. 2.17c are ratios between energies reconstructed in jet-cone and energies of original b-quark produced. It is seen that with increasing jet-cone energy threshold most probable ratio marginally increases, from 0.4 in case of 3 GeV threshold to 0.5 for 5 GeV and 0.6 in case of 10 GeV threshold.

Summary

In this work, I tried to investigate jets containing beauty quark, search for possibility of extracting information about their relative distances, through electrons from electronic decays of b-quarks hadronisation products.

It is obvious that these electrons can approximate their original direction, and help differentiate between b-jets and c-jets, because electrons from charm containing hadrons are not as common at the center of jet than electrons from beauty containing hadrons.

Also it is seen that with increasing energy and transverse momentum of b-quark, probability of its reconstruction increases. From increasing ration of beauty quark's energy reconstructed with increasing threshold for jet-cone energy, it is apparent that with higher energy of beauty quark larger portion of it's energy is reconstructed.

Bibliography

[1] Alessandro B., (ed.) et al., *"ALICE: Physics performance report, volume II ",* J.Phys.G32 (2006) 1295.

[2] Carminati F., et al., *"ALICE: Physics Performance Report, Volume I ",* J.Phys.G30 (2004) 1517.

[3] Cortese P., et al., *"ALICE electromagnetic calorimeter technical design report",* CERNLHCC-2008-014 (2008).

[4] Vajzer M., *"Study of identification of jets containing heavy quark",* bachelor thesis, Czech Technical University in Prague, Faculty of Nuclear Sciences and Physical Engineering (2008).

[5] T. Sjöstrand, S. Mrenna and P. Skands, *JHEP05 (2006) 026*.